Article Title

Impact of diesel-hythane dual-fuel combustion on engine performance and emissions in a heavy-duty engine at low-load condition

Authors:

K. Longo[1], X. Wang[1] and H. Zhao[1]

[1]Centre for Advanced Powertrain and Fuels, Brunel University London, Kingston Lane, Uxbridge, Middlesex, UB8 3PH, UK

Corresponding author:

K. Longo

Email: kevin.longo@brunel.ac.uk

Acknowledgments:

Mr K. Longo acknowledges the Guangxi Yuchai Machinery Company for supporting his PhD study supervised by Prof. Hua Zhao and Dr Xinyan Wang at Brunel University London.

Abstract

Heavy-duty diesel vehicles are currently a significant part of the transportation sector, as well as one of the major sources of carbon dioxide (CO_2) emissions. International commitments to reduce greenhouse gas (GHG) emissions, particularly CO_2 and methane (CH_4) highlight the need to diversify towards cleaner and more sustainable fuels. Hythane, a 20% hydrogen and 80% methane mixture, can be a potential solution to this problem in the near future. This research was focused on an experimental evaluation of partially replacing diesel with hythane fuel in a single-cylinder 2.0 litre heavy-duty diesel engine operating in the diesel-gas dual fuel combustion mode. The study investigated different gas substitution fractions (0%, 38% and 76%) of hythane provided by port fuel injections at 0.6 MPa indicated mean effective pressure (IMEP) and a fixed engine speed of 1200 rpm. Various engine control strategies, such as diesel injection timing optimisation, intake air pressure and exhaust gas recirculation (EGR) were investigated in order to optimise the dual-fuel combustion mode. The results indicated that by using hythane energy fraction (HEF) of 76% combined with 125 kPa intake air boost and 25% EGR dilution, CO_2 emissions could be decreased by up to 23%, while indicated thermal efficiency (ITE) was compromised by 1.5 percentage points, equivalent to a 3% reduction. Furthermore, soot was maintained below Euro VI limit and nitrogen oxides (NOx) level was held below the Euro VI regulation limit of 8.5 g/kWh assuming a NOx conversion efficiency of 95% in a selective catalyst reduction (SCR) system. Nevertheless, carbon monoxide (CO), unburned hydrocarbon (HC) and methane slip levels were considerably higher, compared to the diesel-only baseline. The use of a pre-injection prior to the diesel main injection was essential to control the heat release and pressure rise rates under such conditions.

1. Introduction

Transportation energy demands account for approximately 20% of global energy consumption and are anticipated to rise by 25% between 2019 and 2050. This is due to an expected increase in the number of vehicles, in particular heavy-duty (HD) vehicles as a result of economic growth [1].

According to the Intergovernmental Panel on Climate Change (IPCC) [2], the combustion of fossil fuels is a major contributor to the global warming by releasing substantial concentration of GHG, such as carbon dioxide (CO_2) into the atmosphere. In 2017, HD vehicles were responsible for about 6% of the CO_2 emissions in European Union (EU) [3]. Therefore, this increasing concern about CO_2 has prompted the implementation of new regulations to limit the CO_2 generation in the transportation sector.

Currently, the criterion for the evaluation of internal combustion (IC) engines is their tailpipe emissions [4]. Thereby, a conventional diesel combustion (CDC) engines will thus no longer be able to meet the upcoming strict emission regulations, requiring the employment of new technologies and alternative low and zero carbon fuels. At present, the most intensive research is being conducted on two possibilities. The first is an attempt to completely eliminate the use of fossil fuels in internal combustion engines (ICE), while the second is to burn more efficiently with particular attention to exhaust emissions. The latter has been the most common approach in recent years and has contributed to the substantial reduction in pollutant emissions.

Co-combustion of fuels with different properties, often known as dual-fuel (DF) combustion, are capable of reducing both pollutants and CO_2 emissions when a low carbon fuel is used [5], however, this technology has limited engine operation map, mainly at lower and higher loads due to incomplete or knocking combustion [6]. In particular, diesel-natural gas dual-fuel compression ignition (CI) combustion has been demonstrated as an effective solution for HD applications thanks to their simplicity of adaptation to existing ICEs [7]. Compressed natural gas or bio-gas can be fed through a port fuel injection (PFI) system in a dual-fuel CI engine to provide a lean and homogeneous distribution of the low reactivity fuel in the combustion chamber, resulting in multiple ignition spots [8]. When compared to a diesel-only operation, this method allows for reduced local fuel-air equivalence ratios and combustion temperatures, resulting in lower soot and NOx formation [9]. Another reason for the simultaneous decrease in soot and NOx suggested by Iorio et al. [10] was this combustion mode has a low flame temperature due to a higher ratio of heat capacity of CH_4.

According to Stettler et al. [11], when compared to diesel-only vehicles, lean-burn compressed natural gas (CNG) dual-fuel vehicles reduced CO_2 emissions by up to 9%. This conclusion was obtained after studying the energy consumption, greenhouse gas emissions, and pollutants produced by five aftermarket dual-fuel engine configurations in two vehicle platforms.

In fact, both the diesel injection timing and the properties of low reactivity fuel have a significant impact on DF combustion operation, affecting both engine performance and exhaust emissions [12, 13]. With increasing diesel injection advance, NOx increased while carbon monoxide (CO) and soot emissions were reduced [12]. Moreover, Pedrozo et al. [14] concluded that the combination of reactivity-controlled compression ignition (RCCI) and late intake valve closing (LIVC) can reduce unburned methane and also NOx emissions up to 80% in a diesel-CNG combustion,

Though, due to the properties of methane (CH_4), generally the main compound of natural gas, diesel-CNG dual-fuel combustion has some drawbacks, such as slower flame propagation, which results in longer combustion duration and, as a result, lower efficiency [15]. Also, this combustion mode is accompanied by unburned CH_4 emission, also known as methane slip [14]. CH_4 is a GHG with 27 times global warming potential (GWP) of the CO_2 emission over a 100-year lifetime [16]. Furthermore, the combination of natural gas and diesel enable the DF technology to achieve similar thermal efficiency to that of the conventional diesel engines only at high loads, as reported in [17, 18].

When produced from renewable sources, hydrogen, on the other hand, has no carbon and is a clean and environmentally friendly fuel [19]. Nonetheless, the use of pure hydrogen as a fuel in a DF engine, which provides increased efficiency with respect to the CDC mode, it demonstrates certain limitations on the input energy fraction, due to the problem of pre-ignition and backfire occurring before the diesel fuel injection. Likewise, hydrogen is also associated with other undesirable effect, such as engine knocking owning to its intensity, as reported in [20].

By that, the usage of hydrogen blended with methane, commonly known as hythane, has the potential to mitigate the problems associated with separate methane and hydrogen combustion [15, 21]. The higher reactivity of the hydrogen improves combustion stability, resulting is faster and more complete combustion of methane, and lower unburned CH_4 [22, 21]. Graham et al. [23] indicated that hythane can provide a 10%-20% decrease in GHG levels, namely CO_2 emissions at the tailpipe when compared with diesel. However, this reduction is only relevant when the hydrogen is produced from renewable sources [21]. Therefore, hythane with hydrogen content up to 20% by volume can be deployed with existing CNG infrastructure and on-board gas supply system without significant modification, effectively reducing CO_2 emissions at quite moderate financial costs [21, 24].

De Simio et al. [6] investigated a wide variety of diesel injection timings for diesel DF operation with natural gas and hythane mixtures containing up to 25% hydrogen by volume in a four-cylinder CI light-duty engine at low and medium loads. Although the highest CO_2 reduction and brake thermal efficiency (BTE) combination has been evidenced at very advanced diesel start of injection (SOI) for 72% of hythane energy fraction (HEF) with 15% hydrogen by volume at low engine load, when RCCI DF is deployed, it is possible to reach 20-25% CO_2 reduction at the cost of a roughly 23% drop in BTE for later diesel SOIs (conventional DF). Conversely, equivalent CO_2, which combines CO_2, CH_4 and non-methane HC emissions, has increased significantly when compared to CDC.

Because of the higher flame temperature of hydrogen, NOx concentration increases with higher hydrogen addition, whereas CO and HC levels decrease [25, 26]. Nevertheless, Talibi et al. [15] has noted a different trend by investigating the effect of hythane enrichment with diesel pilot injection in a single-cylinder light-duty CI engine. It was found that CO and HC were significantly higher while employing diesel-hythane dual-fuel (DHDF) mode. Furthermore, a considerable reduction of particulate matter (PM) emissions was achieved compared to CDC. Tutak et al. [27] tested various compositions of hydrogen and CNG in a single-cylinder light-duty diesel engine and concluded that the addition of hydrogen accelerated combustion, shortening the duration of the combustion event. Additionally, it was also found that higher hydrogen and CNG fractions resulted in an increase in peak pressure and temperature as well as higher NOx emissions.

The use of EGR has been proven as an effective method to extend DF operation. This is associated with a reduction in combustion temperature as a result of the increased specific heat capacity and dilution level of the in-cylinder charge [28, 29]. This delays the ignition time of the premixed fuel and hence allows to decrease the levels of PRR and NOx emissions during dual-fuel operation [30]. Moreover, flame stability improves in the presence of EGR at various air-fuel ratios [31, 32]. Nonetheless, Qian et al. [33] conducted a study on a hydrogen-enriched diesel combustion and determined that increasing EGR levels reduced thermal efficiency at all load engine settings. On the other hand, as the combustion temperature reduces as the air-fuel ratio increases, combining hydrogen addition with higher air-fuel ratios, i.e. greater intake air pressures, can lead to a decrease in NOx emissions. [26, 34].

Abdelaal et al. [35] compared CDC and DF modes with and without EGR with 80% diesel replacement (energy basis) at different engine loads in a single-cylinder light-duty natural gas diesel engine. When compared to CDC, DF delivered a considerable reduction in CO_2 emissions at part loads, while thermal efficiency dropped by roughly 13%. HC and CO levels, on the other hand, are higher in DF mode. With the inclusion of 20% EGR, however, it was able to achieve similar thermal efficiency to diesel-only mode without significantly impacting CO_2 levels. And, despite a decrease in HC and CO emissions, their values remained significantly higher than the CDC.

The majority of previous works employing hythane fuel have mainly been focused on small- and light-duty engines, with limited research on heavy-duty engines available. Moreover, studies with considerable high HEF have indicated reasonable CO_2 reduction at the expense of a significant drop in thermal efficiency at part engine loads. Therefore, the current study, which was conducted on a single-cylinder heavy-duty diesel engine with port fuel injected hythane at an engine load of 0.6 MPa indicated mean effective pressure (IMEP), aims to explore the CO_2-ITE trade-off by using a HEF of up to 76%. Advanced engine and combustion control strategies, such as late diesel injection, intake air pressure and EGR dilution were explored to identify the optimum strategies for minimum GHG emissions of CO_2 and CH_4 without harming ITE and NOx emissions. The optimised DHDF results were then compared to the conventional diesel only and a baseline diesel-hythane dual fuel operations.

2. Experimental setup

2.1 Engine setup and specifications

A schematic diagram of the single-cylinder compression ignition engine experimental setup is illustrated in Figure 1. An eddy current dynamometer was used to absorb the power produced by the engine. An external compressor supplied fresh intake air to the engine, which was controlled by a closed-loop system for boost pressure. The intake manifold pressure was precisely controlled by a throttle valve positioned upstream of a surge tank. A thermal mass flow metre was used to measure the air mass flow rate ($\dot{m}_{air}$). A water-cooled heat exchanger was used to regulate the temperature of the boosted air. To mitigate pressure oscillations, another surge tank was installed in the exhaust manifold. The required exhaust manifold pressure was set using an electrically controlled backpressure valve placed downstream of the exhaust surge tank.

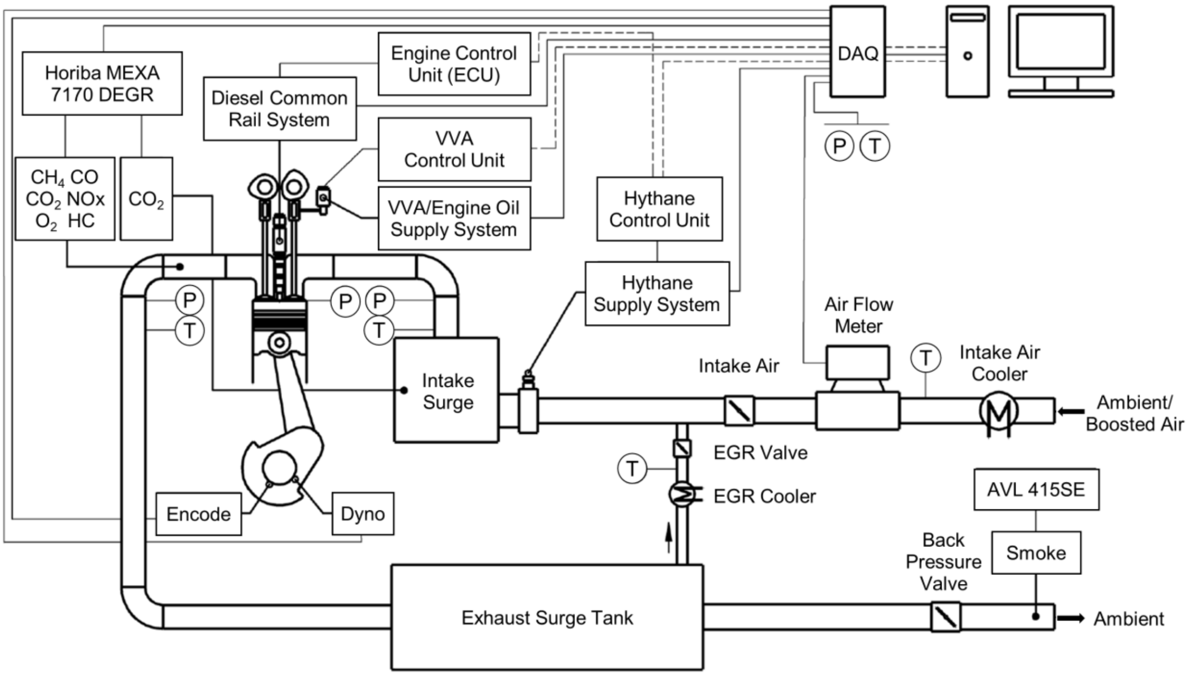

Figure 1. Schematic diagram of the dual-fuel engine experimental setup.

Table 1 shows the HD engine hardware specifications. A 4-valve swirl-oriented cylinder head and a stepped-lip piston bowl design constituted the combustion system. Separate electric motors controlled the coolant and oil pumps. Throughout the experiments, the engine coolant and oil temperatures were set to 80°C, and the oil pressure was kept at 400 kPa.

Table 1. Single-cylinder HD engine specifications.

Parameter	Value
Bore/stroke	129/155 mm
Connecting rod length	256 mm
Displaced volume	2026 cm^3
Clearance volume	128 cm^3
Geometric compression ratio	16.8
Maximum in-cylinder pressure	18 MPa
Piston type	Stepped-lip bowl
Diesel injection system	Bosch common rail, injection pressure of 30-220 MPa, 8 holes, 150° spray
Hythane port fuel injection system	G-Volution controller and two Clean Air Power injectors SP-010, injection pressure of 800kPa

Furthermore, the engine also included a prototype hydraulic lost-motion variable valve actuation (VVA) system on the intake camshaft. This allows for the intake valve closing (IVC) to be adjusted, enabling for a decrease in the effective compression ratio (ECR). This reduces compression pressures and temperatures, as well as the mass trapped in the cylinder at a given boost pressure.

However, in order to simplify the experimental investigation, intake valve timings were kept constant at baseline values throughout the experiments, with its intake valve opening (IVO) at -330 ± 1 crank angle degrees (CAD) and IVC at -187 ± 1 CAD.

2.2 Fuel supply and proprieties

In this study, hythane gas, supplied by British Oxygen Company (BOC) Ltd, was employed as the premixed fuel of the dual-fuel combustion and it is composed of 80% methane and 20% hydrogen gas mixture (molar).

Hythane gas was stored in a rack of six interconnected 20 MPa bottles outside of the engine test cell. Specially developed hoses for the conveyance of CNG have been used, as they are constructed of a conductive nylon core designed to dissipate static build-up. From there, Hythane was fed into a pair of pneumatically controlled safety valves, a high-pressure filter and a high-pressure regulator that dropped the gas pressure to 1 MPa. The pressure regulator was kept constant by the hot engine coolant to counteract the reduction in temperature experienced by the gas during expansion.

After flowing through the high-pressure regulator, hythane was fed into the test cell into an Endress + Hauser Promass 80A Coriolis flow meter. After this mass flow meter, a low-pressure filter, a purge/pressure regulator that adjusted the final hythane pressure to 0.8 MPa, and an emergency shut-off valve were connected, before a flex hose connected the gas stream to the injector block. The injector block, designed for NG application, was installed upstream of the intake surge tank to facilitate the mixing of the fuel gas with the intake air. An injector driver controls the pulse width of the gas injectors and allowed the engine to run at different HEF by altering the hythane mass flow rate ($\dot{m}_{hythane}$).

The high-pressure common rail diesel injection system, which can provide up to three injections per cycle, was controlled by a dedicated engine control unit (ECU). The diesel mass flow rate ($\dot{m}_{diesel}$) was determined using two Endress + Hauser Promass 83A Coriolis flow meters by measuring the total fuel supplied to and from the diesel high-pressure pump and injector.

During the dual-fuel operation, the bulk fuel mass of port fuel injected hythane was ignited by direct injected diesel. Table 2 lists the key properties of the diesel and hythane utilised in this experiment.

Table 2. Fuel proprieties of diesel and hythane.

Property	Unit	Diesel	Hythane
General proprieties			
Lower heating value (LHV)	MJ/kg	42.9	52.1
Stoichiometric air-fuel ratio (AFR)	-	14.5	17.7
Gas density	kg/m^3	-	0.562
Cetane number	-	> 45	< 5
Liquid density (101.325 kPa, 20°C)	kg/dm^3	0.827	-
Normalised fuel's molar mass	g/mol	13.9	16.5
Normalised molecular composition	-	$CH_{1.825}O_{0.0014}$	$CH_{4.492}$
Gas composition (mole fraction)			
Methane (CH_4)	%	-	80.0
Hydrogen (H_2)	%	-	20.0
Fuel contents (mass fraction)			
Carbon (%C_{fuel})	%	86.6	72.6
Hydrogen (%H_{fuel})	%	14.2	27.4
Oxygen (%O_{fuel})	%	0.2	0.0
Calculated carbon intensity			
Mass of CO_2 emissions per mole of fuel	gCO_2/mol	44.0	44.0
Mass of CO_2 emissions per mass of fuel	gCO_2/g	3.2	2.7
Assuming the complete conversion of hydrocarbon fuel into CO_2	gCO_2/MJ	73.9	51.1
Maximum theoretical CO_2 reduction considering a constant ITE	%	-	30.9
Estimated CO_2 reduction with a HEF = 76%	%	-	23.5

An important parameter for the dual-fuel operation is the HEF, which is given by the ratio of the energy content of the hythane injected to the total fuel energy supplied to the engine. As show in Table 2, using a HEF of 76% can minimise exhaust CO_2 emissions by approximately 24% when hydrocarbon fuel is completely converted into CO_2.

$$HEF = \frac{\dot{m}_{hythane} LHV_{hythane}}{\dot{m}_{hythane} LHV_{hythane} + \dot{m}_{diesel} LHV_{diesel}} \quad (1)$$

where: $\dot{m}_{diesel}$ and $\dot{m}_{hythane}$ the mass flow rate of diesel and hythane, respectively; LHV_{diesel} and $LHV_{hythane}$ the lower heating value of diesel and hythane, respectively.

2.3 Exhaust emissions measurements and analysis

An AVL 415SE smoke metre was used to measure the smoke number downstream of the exhaust back pressure valve. The measurement was taken in filter smoke number (FSN). Other exhaust emissions, such as CO_2, CO, CH_4, HC, and NOx, were monitored using a heated line on a Horiba MEXA-7170 DEGR emission analyser located in the exhaust pipe before the exhaust back pressure valve. The concentration of these gaseous emissions in the exhaust stream was measured in parts per million (ppm). All the exhaust gas components were then converted to net indicated specific gas emissions in g/kWh, according to Regulation No. 49 of UN/ECE [36]. The following is an example of the CO_2 conversion calculation:

$$ISCO_2 = \frac{\dot{m}_{CO_2}}{P_{ind}} = \frac{u_{CO_2}\,[CO_2]\,\dot{m}_{exh}}{P_{ind}} \tag{2}$$

where: u_{CO_2} the raw exhaust gas constant; $[CO_2]$ the concentration of CO_2 in ppm; $\dot{m}_{exh}$ the total exhaust mass flow rate; P_{ind} the engine net indicated power calculated from the measured IMEP

The aforementioned regulation also required that NOx and CO emissions be converted to a wet basis by using a raw exhaust gas correction factor that is dependent on the in-cylinder fuel mixture composition. In addition, the measurement of the HC was performed on a wet basis by a heated flame ionisation detector (FID), while CO and CO_2 were measured through a non-dispersive infrared absorption (NDIR). A chemiluminescence detector (CLD) was used to quantify NOx emissions. In this study, the EGR rate was defined as the ratio of the measured CO_2 concentration in the intake surge tank to the CO_2 concentration in the exhaust manifold.

2.4 Data acquisition and analysis

Two National Instruments data acquisition (DAQ) cards linked to a computer were used to acquire the signals from the measurement devices. The crank angle resolution data was sent to a USB-6251 high-speed DAQ card, which was synchronised with an optical encoder with 0.25 CAD resolution. The low-frequency engine operation conditions were recorded using a USB-6210 low-speed DAQ card. An in-house designed DAQ software and combustion analyser displayed this data in real time.

Temperatures and pressures at relevant points were measured using K-type thermocouples and pressure gauges, respectively. Intake and exhaust manifold pressures were measured by two Kistler 4049A water-cooled piezoresistive absolute pressure sensors coupled to Kistler 4622A amplifiers. The in-cylinder pressure was measured by a Kistler 6125C piezoelectric pressure sensor coupled with an AVL FI Piezo charge amplifier.

The crank angle-based in-cylinder pressure traces were averaged over 200 consecutives cycles for each operating point and used to calculate the IMEP. It was also used to obtain the apparent net heat release rate (HRR), following Heywood's equation [37]

$$HRR = \frac{dQ}{d\theta} = \frac{\gamma}{\gamma - 1} p \frac{dV}{d\theta} + \frac{1}{\gamma - 1} V \frac{dp}{d\theta} \tag{3}$$

where: p the in-cylinder pressure; V the in-cylinder volume; γ the ratio of specific heats; θ the CAD.

Due to the fact that the absolute value of the heat released is less essential in this study than the bulk shape of the curve to crank angle, a constant γ of 1.33 was assumed throughout the engine cycle.

The mass fraction burned (MFB) was estimated by the ratio of the integral of the HRR to the maximum cumulative heat release. Combustion phasing was determined by the crank angle of 50% (CA50) MFB. Combustion duration was represented by the period between the crank angle of 10% (CA10) and 90% (CA90) cumulative heat release.

The ignition delay was defined as the period between the start of diesel main injection (SOI_2) into the combustion chamber and the start of combustion (SOC), which was set to 2% MFB. The average in-cylinder pressure and resulting HRR were smoothed using a Savitzky-Golay filter, after the combustion characteristics and ignition delay were estimated.

The pressure rise rate (PRR) was calculated as the average of the maximum pressure variations over 200 cycles of in-cylinder pressure versus crank angle. The coefficient of variation of IMEP (COV_{IMEP}) was determined using the set of IMEP values from the 200 sampled cycles of the test engine.

$$COV_{IMEP} = \frac{\sigma_{IMEP}}{\overline{IMEP}} \times 100\% \tag{4}$$

where: σ_{IMEP} the standard deviation of IMEP; $\overline{\text{IMEP}}$ the mean of IMEP.

The mean in-cylinder gas temperature at any crank angle position was computed using the ideal gas law [37].

The electric current signal sent from the ECU to the diesel injector solenoid was measured using a current probe. The signal was corrected by adding the energising time delay that had previously been measured in a constant volume chamber. The resulting diesel injector current signal allowed the diesel injections be determined.

The indicated thermal efficiency was classified as the ratio of work done to the rate of fuel energy supplied to the engine, as shown below:

$$ITE = \frac{3.6P_{ind}}{\dot{m}_{hythane}LHV_{hythane} + \dot{m}_{diesel}LHV_{diesel}} \tag{5}$$

where: P_{ind} the engine net indicated power calculated from the measured IMEP.

Combustion efficiency calculations were based on the emissions products not fully oxidised during the combustion process except soot as:

$$Combustion\ efficiency = 1 - \frac{P_{ind}}{1000} \times \left[\frac{ISCO\ LHV_{CO} + ISHC\ LHV_{hythane}}{\dot{m}_{hythane}LHV_{hythane} + \dot{m}_{diesel}LHV_{diesel}}\right] \tag{6}$$

where: LHV_{CO} is equivalent to 10.1 MJ/kg [37].

Combustion losses associated with HC emissions were thought to be caused entirely by unburned hythane fuel. This is a conservative approach since the $LHV_{hythane}$ is higher than the LHV_{diesel}.

Finally, the relative air-fuel ratio (λ) was determined as follows:

$$\lambda = \frac{\dot{m}_{air}}{\dot{m}_{hythane}AFR_{hythane} + \dot{m}_{diesel}AFR_{diesel}} \tag{7}$$

where: $AFR_{hythane}$ and AFR_{diesel} the stoichiometric air-fuel ratio of hythane and diesel, respectively.

2.5 Instrumentation specifications

Finally, before conducting the experiments, all of the instruments utilised are tested and calibrated under the same operating conditions as the actual tests in order to ensure measurement accuracy. Table 3 summarises all of the measurement instruments used during the experiments, as well as the measurement range values and accuracy.

Table 3. Test cell measurement devices

Variable	Manufacturer	Device	Measurement range	Linearity/Accuracy
Speed	Froude Hofmann	AG 150 dynamometer	0-8000 rpm	±1 rpm
Torque	Froude Hofmann	AG 150 dynamometer	0-500 Nm	±0.25% of FS
Clock Signal	Encoder Technology	EB58	0-25000 rpm	0.25 CAD
Diesel flow rate (supply)	Endress+Hauser	Proline Promass 83A02	0-20 kg/h	±0.10% of reading
Diesel flow rate (return)	Endress+Hauser	Proline Promass 83A01	0-100 kg/h	±0.10% of reading
Hythane flow rate	Endress+Hauser	Proline Promass 80A02	0-20 kg/h	±0.15% of reading
Intake air mass flow rate	Endress+Hauser	Proline T-mass 65F	0-910 kg/h	±1.5% of reading
In-cylinder pressure	Kistler	Piezoelectric pressure sensor Type 6125C	0-30 MPa	≤ ±0.4% of FS
Intake and exhaust pressures	Kistler	Piezoresistive pressure sensor Type 4049A	0-1 MPa	≤ ±0.5% of FS

Oil pressure	GE	Pressure transducer UNIK 5000	0-1 MPa	< ±0.2% of FS
Temperature	RS	Thermocouple K Type	233-1473 K	≤ ±2.5 K
Fuel injector current signal	LEM	Current probe PR30	0-20 A	±2 mA
Smoke number	AVL	415SE	0-10 FSN	-
CO	Horiba	MEXA-7170-DEGR (Non-Dispersive Infrared Detector)	0-12 vol%	≤ ±1.0% of FS or ±2.0% of readings
CO_2	Horiba	MEXA-7170-DEGR (Non-Dispersive Infrared Detector)	0-20 vol%	≤ ±1.0% of FS or ±2.0% of readings
HC	Horiba	MEXA-7170-DEGR (Heated Flame Ionization Detector)	0-500 ppm or 0-50k ppm	≤ ±1.0% of FS or ±2.0% of readings
CH_4	Horiba	MEXA-7170-DEGR (Non-Methane Cutter + Heated Flame Ionization Detector)	0-0.25k ppm or 0-25k ppm	≤ ±1.0% of FS or ±2.0% of readings
NO/NOx	Horiba	MEXA-7170-DEGR (Heated Chemiluminescence Detector)	0-500 ppm or 0-10k ppm	≤ ±1.0% of FS or ±2.0% of readings
EGR	Horiba	MEXA-7170-DEGR (Non-Dispersive Infrared Detector)	0-20 vol%	≤ ±1.0% of FS or ±2.0% of readings

3. Test methodology

The experimental testing was carried out at a constant engine speed of 1200 rpm and a fixed load of 0.6 MPa IMEP, which is equivalent to 25% of the full engine load and, represents a high residency area in a typical HD vehicle drive cycle, such as WHSC, and indicated in Figure 2.

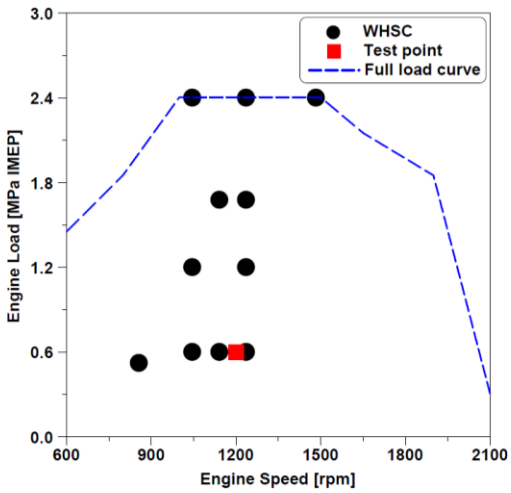

Figure 2. The selected test point over the experimental HD engine speed-load map.

Table 4 summarises the engine test conditions for the CDC, baseline DHDF and optimised DHDF operation modes. The first part of the experiments comprised a comparison on engine emissions and performance between the two aforementioned combustion modes by varying the HEF. This comparison was carried out using a constant baseline late diesel injection. Both COV_{IMEP} and PRR were used to define the HEF limit, which was approximately 76%, resulting in an overall combustion mixture of 24% diesel, 61% methane, and 15% hydrogen. Also, the intake and exhaust air pressure set-points from a Euro V compliant multi-cylinder HD diesel engine were used in order to provide a sensible starting point.

Other experiments were carried out to obtain the engine calibration for optimised DHDF combustion mode with the highest HEF. This optimisation included the sweep of several engine control parameters, namely diesel injections timing, intake air pressure (P_{int}), and EGR rate. As a result, an optimal point was reached that achieved with the best trade-off between the GHG emissions (CO_2 and CH_4) and the ITE whilst keeping the engine-out NOx of less than 8.5 g/kWh. This NOx level was necessary in order to achieve a Euro VI emissions compliance with a NOx conversion of approximately 95% in the SCR system.

Throughout the experiments, exhaust pressures were adjusted to provide a constant pressure differential of 10 kPa above the intake air pressure to achieve a fair comparison with equivalent pumping work and to realise the required EGR rate. Intake air temperature was maintained constant at 35°C during all the experiments by using an air-to-water cooler and intake air heater. A diesel pre-injection (SOI_1) with an estimated volume of 3 mm^3 and a constant delay time of 1.1ms (7.92 CAD at 1200 rpm) before SOI_2 was employed to reduce the levels of PRR. Moreover, the diesel main injection timings were optimised to achieve the highest ITE in DHDF combustion mode. However, it is worth noting that during this optimisation, the hythane supply was maintained constant while the diesel was automatically adjusted by the ECU in order to achieve the same IMEP, resulting in a slightly HEF variation (around 4%). The limits of the highest average in-cylinder pressure (P_{max}) and the maximum PRR were set to 18 MPa and 2.0 MPa/CAD, respectively. Finally, the COV_{IMEP} of 3% limit was used to determine stable engine operation.

Table 4. Engine testing conditions.

Parameter	Unit	CDC	Baseline DHDF	Optimised DHDF
Engine load (IMEP)	MPa	0.6	0.6	0.6
Engine speed	rpm	1200	1200	1200
Diesel injection strategy	-	Pre- and main injection	Pre- and main injection	Pre- and main injection
Diesel SOI_2	CAD ATDC	-5	-5	Sweep
Diesel injection pressure	MPa	100	100	100
Intake air pressure (P_{int})	kPa	125	125	Sweep
Exhaust air pressure	kPa	135	135	Sweep
Intake air temperature	°C	35 ± 1	35 ± 1	35 ± 1
ECR	-	16.8	16.8	16.8
HEF	%	0	Sweep	~76
EGR	%	0	0	Sweep

Regarding the control of GHG and pollutant emissions from DF combustion engines, Regulation No. 49 of the United Nations Economic Commission for Europe (UN/ECE) [36] enhances the Euro VI emissions standards for on-road HD vehicles by establishing five different types of dual-fuel engines. For the sake of clarity, this study will focus on the evaluation of Type 2B heavy-duty dual-fuel (HDDF) engines. These operate in the hot section of the World Harmonised Transient Driving Cycle (WHTC), with an average gas energy fraction (GEF_{WHTC}) ranging from 10% to 90%, while still enabling for diesel-only engine operation.

The Euro VI emissions standards for Type 2B HDDF engines are shown in Table 5 for both the stationary (WHSC) and transient (WHTC) test cycles. It is worth noting that, with the exception of the HEF experiment, all optimised DHDF experiments used the highest HEF with the goal of maximising hythane utilisation, which contributed to achieve a GEF_{WHTC} of more than 68%.

Table 5. Euro VI emissions limits for Type 2B heavy-duty dual-fuel engines

Emission	Unit	WHSC	WHTC ($GEF\%_{WHTC}$ > 68%)
Nitrogen oxides (NOx)	g/kWh	0.40	0.46
Carbon monoxide (CO)	g/kWh	1.50	4.00
Particulate matter (PM)	g/kWh	0.01	0.01
Total unburned hydrocarbon (HC)	g/kWh	0.13	-
Methane (CH_4)	g/kWh	-	0.50

4. Results and discussion

The results and discussion section examines the impact of hythane addition at a baseline DHDF for various substitution ratios, as well as the optimisation of the DHDF mode for the highest diesel percentage replacement, which includes diesel injection timing, intake air pressure, and EGR rate sweeps. A comparison of CDC, baseline, and optimised DHDF operations is discussed at the end of this section.

4.1 The impact of HEF

In this study, a baseline diesel main injection at -5 CAD ATDC (after top dead centre) with a small diesel pre-injection to attenuate COV_{IMEP} and PRR were employed for different HEF, varying from 0% (diesel-only) to a maximum value of 76%. Because of the exponential growth of PRR, which caused strong knocking, unstable combustion (high COV_{IMEP}) was observed for HEF higher than 76%. Additionally, this experiment was performed without EGR and with a constant intake air pressure of 125 kPa.

Table 6 shows the engine performance, combustion characteristics and indicated specific exhaust emissions whereas Figure 3 depicts the in-cylinder pressure, mean in-cylinder gas temperature, HRR and MFB traces, for CDC and DHDF operations. As seen in Table 6, increasing the HEF resulted in a 15% reduction in CO_2 emissions for a HEF of 76%. This was expected of the addition of hydrogen into the combustion, because the low reactivity port injected fuel has a lower carbon composition (lower C to H ratio) than diesel, as shown in Table 2. Nonetheless, methane slip rose dramatically as HEF increased. This was mainly attributed to the two following reasons. First, hythane is mainly composed by methane, resulting in increased unburned CH_4 levels in the exhaust pipe from the crevices. Second, the inclusion of hythane resulted in a longer ignition delay, in other words, a later SOC, due to the fact that the premixed charge has a lower cetane number comparing to CDC. This aspect, combined with the slower flame propagation speed of methane that results in incomplete and longer combustion duration (CA10-CA90) [7], and a lower and longer HRR peak (Figure 3), resulting in an increase in unburned CH_4 and HC, and as a consequence, a reduction of combustion efficiency [15]. The slower combustion rate can be seen in the MFB trace, which is also shown in Figure 3, with a clear delay of CA50. This lower combustion efficiency had a direct impact on the loss in ITE of roughly 5 percentage points at 76% HEF. In addition, the increase of CO formation for higher rates of diesel replacement is explained by the unburned fuel generated from incomplete combustion, which led to lower mean in-cylinder gas temperature.

Moreover, a minor increase in NOx was seen with increasing HEF percentage. This is explained in part by the presence of hydrogen, which has a higher flame temperature, resulting in a higher peak in-cylinder gas temperature, as shown in Figure 3. As the result, DHDF produced higher exhaust temperature. Specifically, the DHDF operation with 76% HEF yielded a higher exhaust gas temperature (EGT) by about 32°C higher than that measured for CDC. This level of temperature is more favourable for the methane oxidation catalyst (MOC) used in DF engines, since the device typically requires an EGT of more than 400°C for high CH_4 conversion efficiency, and hence a reduction in methane slip [38, 39]. Furthermore, at the maximum HEF, soot emissions were slightly reduced, as shown in Table 6. This is likely because diesel fuel contributed for only 24% of total energy supplied to the engine, resulting in lower local fuel-air equivalence ratios [9].

In terms of the combustion process, Figure 3 indicates that increasing the HEF resulted in a decrease in the in-cylinder pressure. This can be explained by the slower propagation speed of methane [7], the major compound in the mixture. However, it was observed in Figure 3 that the peak of HRR in DHDF was earlier than that in CDC. And on this event, the addition of hydrogen can possibly increase the reactivity of the fuel mixture, leading to earlier peak of the heat release rate. In addition, it can be seen that there was a small heat release of the pre-injected diesel (SOI_1) before SOI_2, which was visible only in the DF combustion mode. This can be further explained by the increased reactivity of the fuel mixture by adding hydrogen.

Table 6. The impact of HEF on low engine load operation.

Parameter	Unit	HEF = 0%	HEF = ~38%	HEF = ~76%
SOI_2	CAD ATDC	-5	-5	-5
COV_{IMEP}	%	2.07	2.37	2.54
PRR	MPa/CAD	0.55	0.56	0.44
P_{max}	MPa	7.54	7.38	6.85
EGT	°C	359	385	391
SOC-SOI_2	CAD	6.4	6.8	7.2
SOC	CAD ATDC	0.9	1.3	1.7
CA50	CAD ATDC	9.1	9.2	11.4
CA10-CA90	CAD	21.1	24.6	25.2
λ	-	2.60	2.39	2.22
ITE	%	44.2	41.0	39.7
Combustion Efficiency	%	99.5	95.4	92.9
$ISCO_2$	g/kWh	666	621	566
$ISCH_4$	g/kWh	0.0	7.6	12.0
ISNOx	g/kWh	7.7	8.6	8.9
ISsoot	g/kWh	0.0169	0.0193	0.0152
ISCO	g/kWh	1.2	7.7	9.0
ISHC	g/kWh	0.7	7.0	11.2

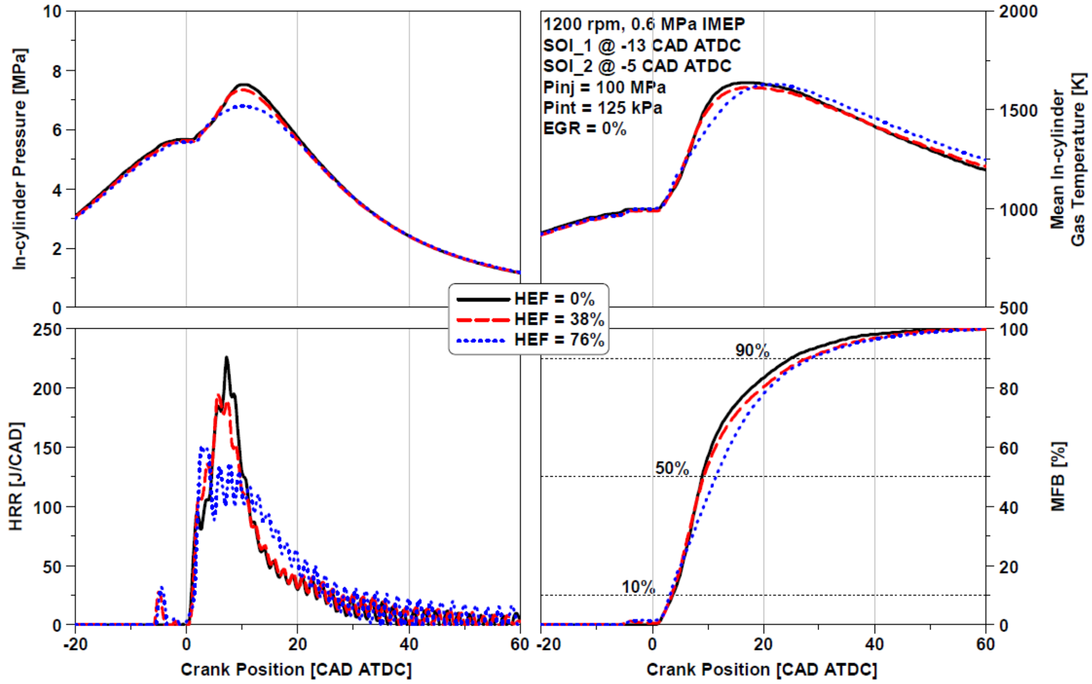

Figure 3. In-cylinder pressure, mean in-cylinder gas temperature, HHR and MFB for low engine load operation with various HEF.

4.2 The effect of SOI_2

In this study, diesel injection timing was investigated in order to analyse its influence on exhaust emissions and engine performance with 76% HEF. Diesel pre- and main injections were used in a DHDF engine. The experiment was performed without EGR and with a constant intake air pressure of 125 kPa.

Figure 4 show indicated specific exhaust emissions, engine performance and combustion characteristics for different HEF respectively, while the in-cylinder pressure, mean in-cylinder gas temperature, HRR and MFB traces of 3 different SOI_2 at approximately 76% HEF were depicted in Figure 5.

Although CO_2 emissions decreased with more advanced SOI 2, which can be explained in part by a shorter combustion period near top dead centre (TDC), the main reason was the lower diesel consumption. This smaller $ISFC_{diesel}$, as seen in Figure 4, can be explained by the ECU's automatic diesel amount adjustment to maintain IMEP constant, since the hythane supply was held constant during the diesel injection sweep, resulting in a slight HEF variation. This increase in diesel amount at late injection timings, on the other hand, contributed to higher combustion efficiency by enhancing the combustion process. Besides, more advanced timings improved the homogeneity of the in-cylinder charge, leading in lower CO and soot levels [12]. By using more advanced SOI_2, both pressure and temperature were significantly increased as shown in Figure 5, which increased NOx emissions but also improved reduced unburned fuel (HC and CH_4) at the end of combustion, and hence improving combustion efficiency.

Delaying the diesel injection, on the other hand, retarded the combustion phasing, resulting in a longer CA10-CA90. As a result, both the ITE and the in-cylinder pressure decreased. However, it is noted that the peak thermal efficiency was obtained at intermediate injection timing, due to optimised combustion phasing as indicated by the values of CA50. As a conclusion, more advanced SOI_2 demonstrated lower carbon emissions and higher engine performance, being -11 CAD ATDC the best timing to optimal trade-off between indicated thermal efficiency and carbon emissions. It allowed for a reduction in CO_2 of 44.6 g/kWh, corresponding to an 8% drop, and a reduction in CH_4 of 0.3 g/kWh, equivalent to a 3% reduction. The ITE was also increased by roughly 2 percentage points. Likewise, at this SOI_2 timing, soot emissions were reduced by about 55%, maintaining them below Euro VI limits. Despite this, EGT dropped as SOI_2 advanced, moving away from the optimal temperature of the MOC in order to achieve high CH_4 conversion efficiency.

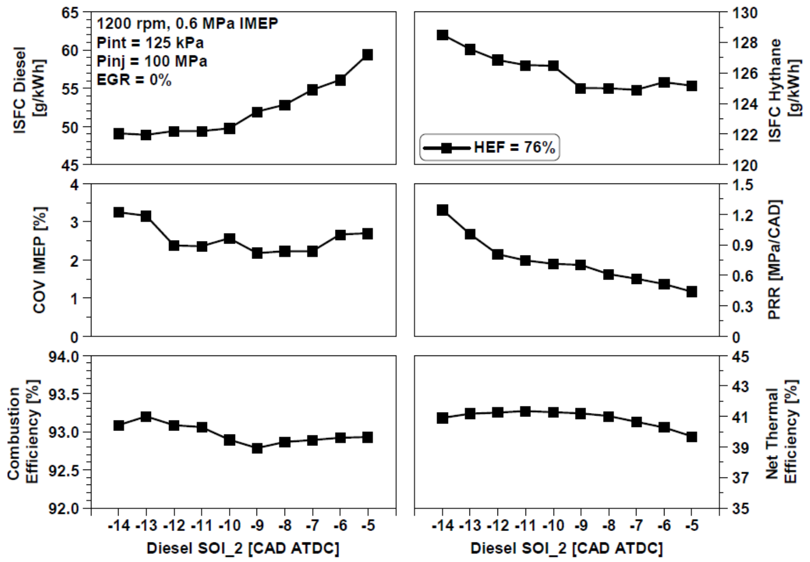

(a)

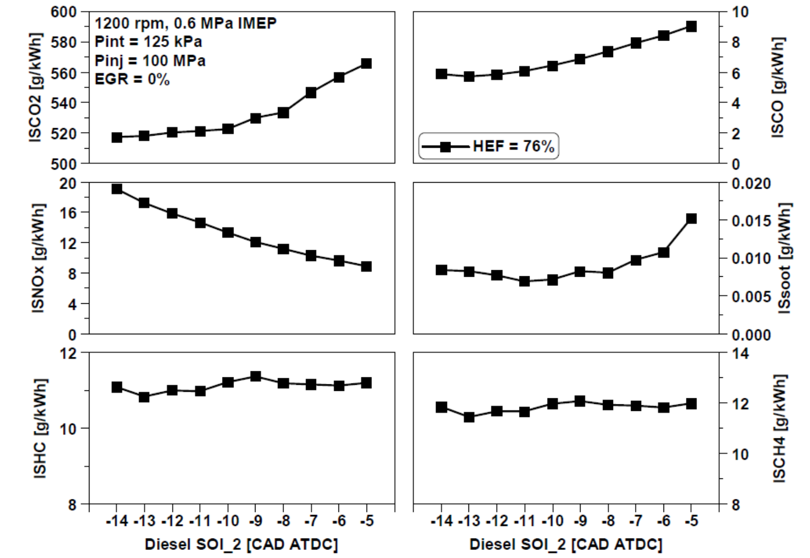

(b)

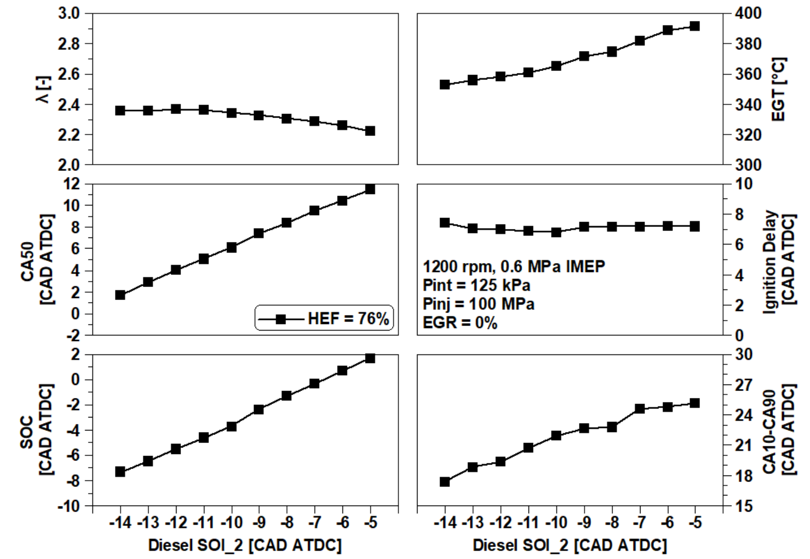

(c)

Figure 4. Effect of diesel SOI_2 at low engine load DHDF operation on: (a) engine performance, (b) net indicated specific exhaust emissions and (c) combustion characteristics.

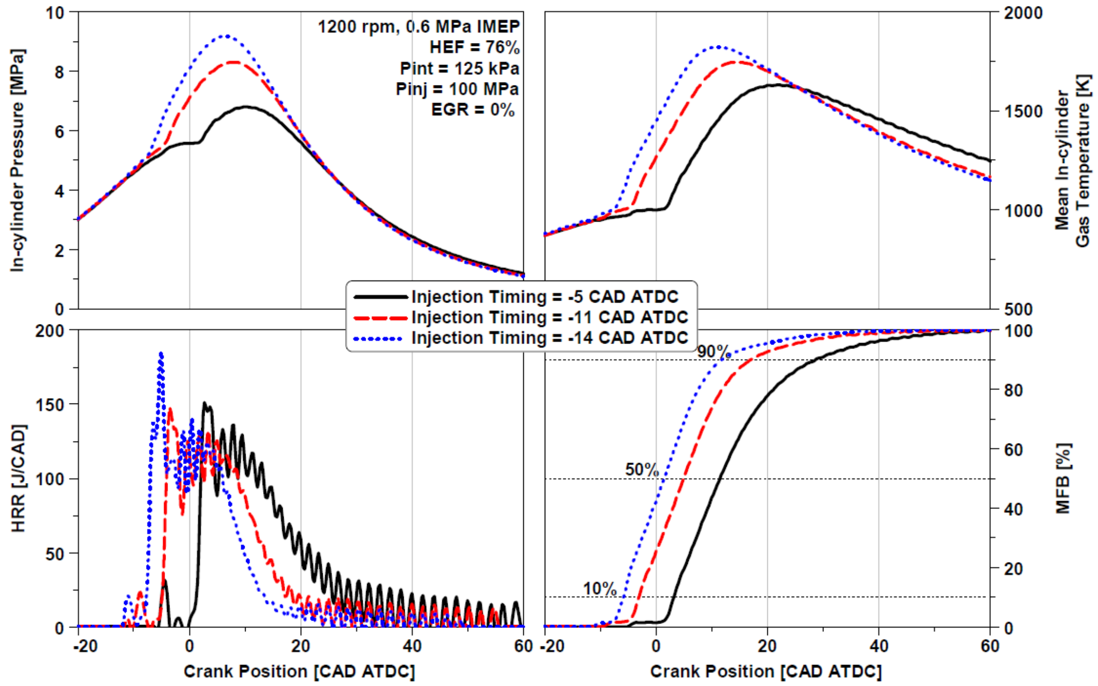

Figure 5. In-cylinder pressure, mean in-cylinder gas temperature, HHR and MFB for low engine load DHDF operation with various diesel SOI_2 at 76% HEF.

4.3 The effect of intake air pressure

Following the studies of DHDF with different injection timings, intake air pressure was swept for 3 different pressures at 76% HEF: 125 kPa, 135 kPa and 145 kPa. EGR was not used in this experiment and diesel injection timing was kept constant at -11 CAD ATDC, which corresponded to the optimised timing achieved in the previous experiment.

The combustion characteristics, performance and exhaust emissions results for the intake pressure sweep are summarised in Table 7, whereas Figure 6 depicts the in-cylinder pressure, mean in-cylinder gas temperature, HRR and MFB traces of this experiment.

Table 7. The effect of P_{int} on low engine load DHDF operation.

Parameter	Unit	P_{int} = 125 kPa	P_{int} = 135 kPa	P_{int} = 145 kPa
HEF	%	76	76	76
SOI_2	CAD ATDC	-11	-11	-11
COV_{IMEP}	%	2.33	3.12	2.35
PRR	MPa/CAD	0.73	0.78	0.62
P_{max}	MPa	8.39	8.80	9.10
EGT	°C	363	341	326
SOC-SOI_2	CAD	6.5	6.3	6.1
SOC	CAD ATDC	-5.0	-5.2	-5.4
CA50	CAD ATDC	4.8	4.8	5.0
CA10-CA90	CAD	19.2	20.6	21.4
λ	-	2.29	2.50	2.68
ITE	%	41.0	40.5	39.7
Combustion Efficiency	%	93.2	91.8	90.9
$ISFC_{diesel}$	g/kWh	52.5	54.6	57.8
$ISFC_{hythane}$	g/kWh	127.5	127.9	128.8
$ISCO_2$	g/kWh	517	519	530
$ISCH_4$	g/kWh	11.3	14.0	15.6
ISNOx	g/kWh	14.9	14.6	14.4
ISsoot	g/kWh	0.0071	0.0118	0.0086
ISCO	g/kWh	5.9	7.4	9.0
ISHC	g/kWh	11.0	13.5	15.1

Higher intake air pressures allowed for more air dilution of the charge in the combustion chamber, resulting in a leaner and lower reactivity mixture (higher λ). This, however, resulted in poor ignition and more incomplete combustion, leading to a longer CA10-CA90 and thus more unburned fuel (HC and CH_4). This resulted in a drop in combustion efficiency as well as a 1.3 percentage point loss in ITE for the highest P_{int}, as shown in Table 7. Albeit the decreased amount of burned fuel led in a slightly decrease in CO_2 ppm, $ISCO_2$ increased when P_{int} was increased due to lower ITE. On the other hand, CO also suffered an increase with higher P_{int}. One possible reason is that incomplete combustion (longer CA10-CA90) generates more CO because CO does not have enough time to oxidise and form CO_2 [40]. Another reason can be the lower in-cylinder combustion temperatures noticed for higher P_{int} due to higher relative air-fuel ratios, since CO formation is also function of mixture temperatures [35, 6]. However, the higher air dilution of the charge for higher intake air pressures increased the heat capacity ratio, allowing the peak in-cylinder gas temperature to be reduced, as shown in Figure 6, resulting in lower NOx formation [26, 34].

Additionally, the longer combustion process is believed to be responsible for the $ISFC_{diesel}$ increase of around 4% and 10% for P_{int} of 135 kPa and 145 kPa, respectively. It is noted that the intake pressure of 125 kPa provided the best compromised between performance and carbon emissions.

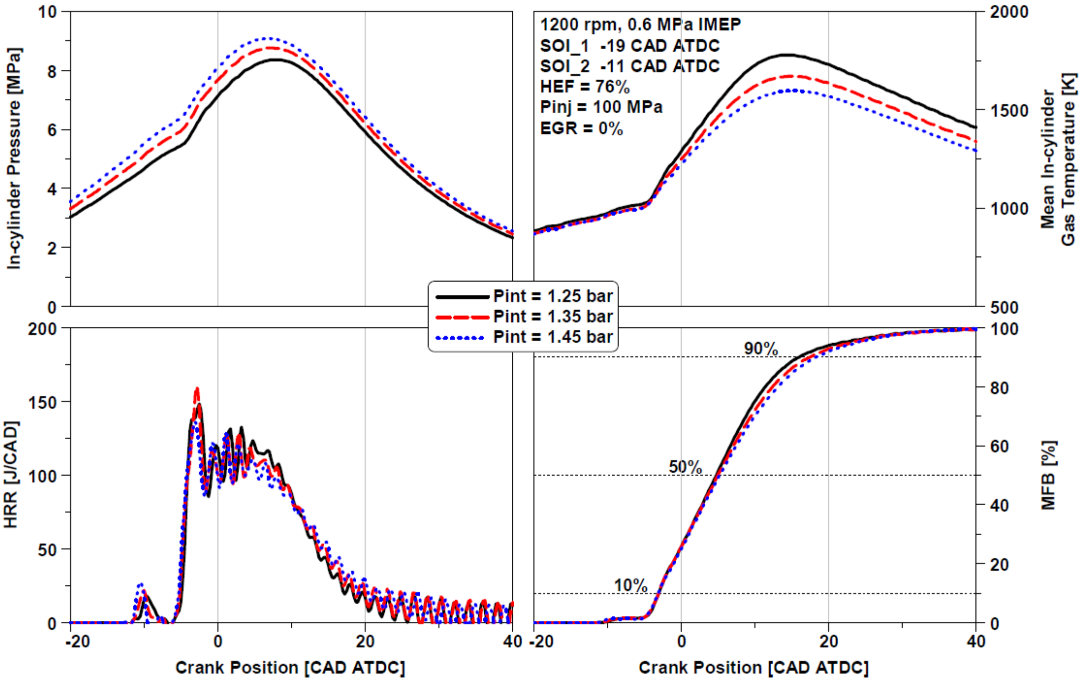

Figure 6. In-cylinder pressure, mean in-cylinder gas temperature, HHR and MFB for low engine load DHDF operation with various Pint.

4.4 The effect of EGR

The last approach used in this study to optimise DHDF for the highest HEF operation was the sweep of EGR rate up to 30%, as shown in Table 8. SOI_2 and P_{int} were kept constant at -11 CAD ATDC and 125 kPa, respectively, which corresponded to the optimised values achieved in the previous experiments. The combustion characteristics, performance and exhaust emissions results for EGR rate sweep are summarised in Table 8, while Figure 7 depicts the in-cylinder pressure, mean in-cylinder gas temperature, HRR and MFB traces of this experiment.

The increase in EGR rate produced lower oxygen concentration and higher heat capacity in the in-cylinder charge, resulting in a slightly longer ignition delay. The longer ignition delay, on the other hand, resulted in a more homogeneous in-cylinder charge, resulting in a higher first HRR peak, as shown in Fig. 9. In addition, the utilisation of EGR extended the combustion duration. As a result, CA50 was delayed, indicating that there was room to optimise SOI_2 for more advanced timing when EGR was employed [41].

The increased in-cylinder temperature, as shown in Figure 7, contributed to a little reduction in CO and HC emissions as well as methane slip, resulting in more complete combustion, in other words, higher combustion efficiency. This is because with EGR, a portion of the unburned fuel (HC and CH_4) is recirculated and reburned in the mixture, due to the presence of a sufficient amount of oxygen in the combustion chamber [35]. As the result, diesel and hythane ISFC will be lower, leading to an improvement in the ITE and minor CO_2 reduction.

However, at 30% EGR rate, a reverse effect was found, resulting in an increase in CO, HC, and CH_4, while soot emissions exceeded the Euro VI limit. This can be due to a lack of oxygen, resulting in poor combustion and more unburned fuel. Therefore, the effectiveness of EGR to reduce HC, CO, and CH_4 emissions by reburning some of the unburned fuel is dependent on the availability of oxygen in the combustion chamber [35].

The NOx emissions were dramatically reduced from 14.9 to 3.1 g/kWh with 30% EGR while the soot emissions were slightly increased due to the reduction in the in-cylinder air-fuel ratio.

As a conclusion, it can be stated with a degree of confidence that EGR of 25% provided the best trade-off between exhaust emissions and efficiency.

Table 8. The effect of EGR on low engine load DHDF operation.

Parameter	Unit	EGR = 0%	EGR = 10%	EGR = 20%	EGR = 25 %	EGR = 30%
HEF	%	76	76	76	76	76
SOI_2	CAD ATDC	-11	-11	-11	-11	-11
COV_{IMEP}	%	1.76	1.52	1.61	1.56	1.76
PRR	MPa/CAD	0.75	0.70	0.62	0.58	0.61
P_{max}	MPa	8.61	8.46	8.44	8.35	8.32
EGT	°C	361	363	367	368	369
SOC-SOI_2	CAD	6.4	6.5	7.2	7.4	7.5
SOC	CAD ATDC	-5.1	-5.0	-4.3	-4.1	-4.0
CA50	CAD ATDC	4.5	4.8	5.1	5.3	5.4
CA10-CA90	CAD	19.1	19.2	19.3	19.6	19.7
λ	-	2.42	2.12	1.95	1.87	1.78
ITE	%	41.1	41.5	42.4	42.7	42.8
Combustion Efficiency	%	93.2	94.0	94.1	94.4	94.3
$ISFC_{diesel}$	g/kWh	50.7	47.6	45.0	43.8	43.8
$ISFC_{hythane}$	g/kWh	121.2	121.1	121.0	120.4	120.1
$ISCO_2$	g/kWh	517.1	518.4	513.9	513.1	513.8
$ISCH_4$	g/kWh	10.9	9.9	9.0	8.4	8.6
ISNOx	g/kWh	14.9	10.4	6.4	4.3	3.1
ISsoot	g/kWh	0.0071	0.0081	0.0093	0.0098	0.0128
ISCO	g/kWh	6.0	5.6	4.9	4.8	4.9
ISHC	g/kWh	10.5	9.5	8.8	8.2	8.4

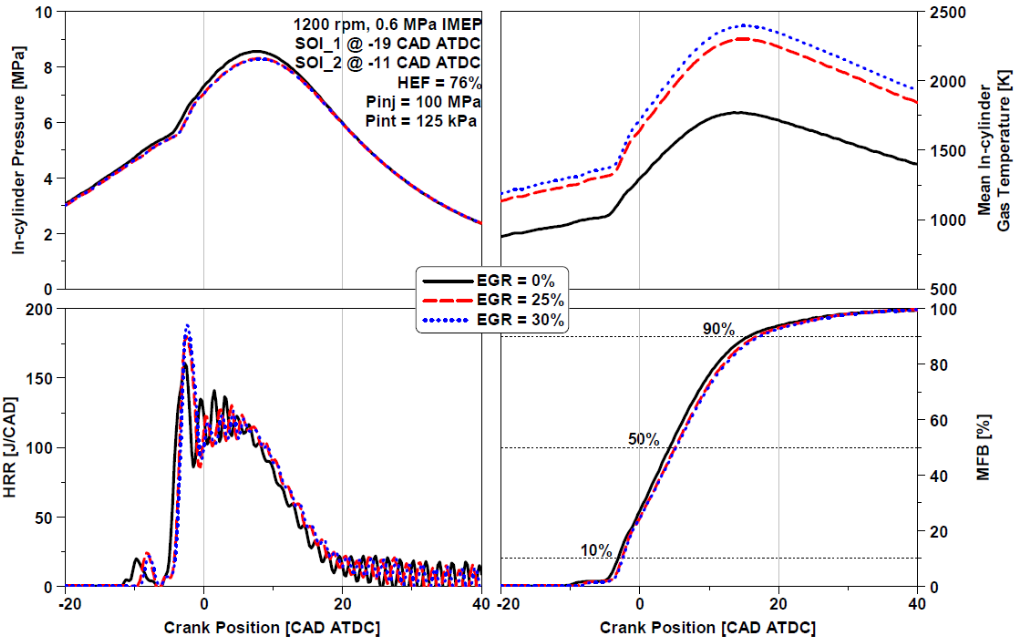

Figure 7. In-cylinder pressure, mean in-cylinder gas temperature, HHR and MFB for low engine load DHDF operation with various EGR.

4.5 Comparison of different engine combustion modes

This section compares the three different combustion modes employed in this study to demonstrate the impact of baseline DHDF and optimised DHDF on engine performance and exhaust emissions at low engine load. Table 9 shows that 76% HEF in a baseline DHDF lowered CO_2 emissions by 15%. The addition of hythane, on the other hand, reduced ITE while elevating methane slip, CO, and HC, which led to a 7% reduction in combustion efficiency. Despite this, optimising DHDF combustion using advanced engine control strategies, such as low booster pressure, diesel injection optimisation, and EGR dilution might mitigate the aforementioned negative effects.

With this optimisation of DHDF, the CO_2 was reduced by 23% when compared to CDC, which is consistent with the estimated CO_2 reduction provided in Table 2, as well as the CO_2 reduction achieved by the literature review, while thermal efficiency was compromised by only 1.5 percentage points (approximately 3%) when compared to conventional diesel combustion. This is an effective result for low engine load conditions when compared to some literature review presented in the Introduction Section. Likewise, NOx emission and soot emissions were reduced by 44% and 42%, respectively. On the other hand, since CH_4 emissions have increased significantly, and taking into account that 1 g of methane in the exhaust gas is equivalent to 27 g of CO_2 over 100 years (IPCC Sixth Assessment Report) [16], methane has offset the carbon reduction provided by the optimised DHDF, yielding 11% more equivalent CO_2 (overall GHG emissions) than the CDC mode. Despite the overall GHG levels increase, it still represents an improvement over what De Simio et al. [6] reported. As a result, methane slip control is essential to keep DHDF mode as a viable solution to reduce real (equivalent) CO_2 emissions from ICEs. MOC are commonly employed with DF engines to oxidise unburned CH_4, although it may be difficult to obtain high methane conversion efficiency at part engine loads due to its light-off temperature (about 400°C), which is still roughly 30°C higher than the EGT achieved by the optimised DHDF regime. Hence, additional optimisation, such as the LIVC strategy [14], is needed to meet the MOC temperature requirement. The use of LIVC may also help to improve the flammability of the in-cylinder charge [14], which may result in higher combustion temperatures and reduced HC and CO. Moreover, CO levels can be greatly reduced by applying a simple oxidation catalyst in the exhaust line [6].

In summary, DHDF optimisation indicated an increase in combustion efficiency when compared to its baseline DF, resulting in a more complete combustion. Despite the fact that CO, HC, and CH4 levels remain high, this optimisation indicates a positive trend of reducing undesired engine-out emissions and shows that there is still room for improvement, making this DF operation a possible viable solution for short-term applications.

Table 9. Comparison of engine efficiencies and emission for three combustion modes

Parameter	Unit	CDC	Baseline DHDF		Optimised DHDF	
ITE	%	44.2	39.7	(-10%)	42.7	(-3%)
Combustion Efficiency	%	99.5	92.9	(-7%)	94.4	(-5%)
$ISCO_2$ equivalent	g/kWh	666	890	(+34%)	740	(+11%)
$ISCO_2$	g/kWh	666	566	(-15%)	513	(-23%)
$ISCH_4$	g/kWh	0.0	12.0	(+1614%)	8.4	(+1100%)
ISNOx	g/kWh	7.7	8.9	(+16%)	4.3	(-44%)
ISsoot	g/kWh	0.0169	0.0152	(-10%)	0.0098	(-42%)
ISCO	g/kWh	1.2	9.0	(+650%)	4.8	(+300%)
ISHC	g/kWh	0.7	11.2	(+1500%)	8.2	(+1071%)

Conclusions

In this study, engine experiments were conducted to demonstrate the capability of advanced engine combustion control strategy to enable significant increase in the replacement of diesel fuel with hythane at a relatively low engine load in order to improve the CO_2-thermal efficiency trade-off in heavy-duty engines. Testing was carried out with port fuel injection of hythane, containing 20% hydrogen and 80% methane molar basis, on a single-cylinder heavy-duty diesel engine operating at a constant engine speed of 1200 rpm and 0.6 MPa IMEP, a typical part-load operating condition of 25% of total engine load. The hythane energy fraction (HEF) was held at 76% ± 1% while dual-fuel combustion mode was optimised for the best trade-off between the lowest CO_2/CH_4 and the highest ITE possible, whilst keeping the NOx emission low. Engine control strategies, such as intake air boosting, diesel injection strategy and EGR addition were explored to identify and achieve an optimised diesel-hythane dual-fuel (DHDF) combustion operation. The main findings can be summarised as follows:

1. The baseline DHDF combustion mode using 76% hythane energy fraction demonstrated a further reduction in CO_2 emissions by 15% when compared to the CDC under the same combustion operating conditions. This was due to the lower C to H ratio of hythane than diesel fuel, which was influenced by the mixture's hydrogen content. However, this was accompanied with a 10% drop (5 percentage points) in the ITE as well as an increase in CO and unburned HC and CH_4 due to incomplete combustion. Soot emissions, on the other hand, were lowered by around 10% to remain within the Euro VI standard due to lower local fuel-air equivalence ratios caused by the replacement of diesel fuel in the in-cylinder mixture.
2. More advanced diesel injection timings resulted in a considerable reduction in CO_2 emissions as well as lower CO and soot levels due to a shorter combustion duration around TDC, which improved in-cylinder mixture reactivity by promoting the fast burning rate of hydrogen. SOI_2 at -11 CAD ATDC provided the best balance of ITE and carbon emissions. As a result, CO_2 emission was decreased by 44.6 g/kWh, reflecting an 8% drop, and a reduction in methane slip of 0.3 g/kWh, equivalent to a 3% reduction.
3. Increase in the intake air pressure led to lower reactivity of the in-cylinder charge, causing poor ignition and incomplete combustion, resulting in slightly higher CO and CO_2 levels and a substantial increase of unburned HC and methane slip (from 11.3 to 15.6 g/kWh). Consequently, both combustion and indicated thermal efficiencies fell by about 2.3 and 1.3 percentage points, respectively.
4. The introduction of 25% EGR significantly reduced the NOx emissions from 14.9 to 4.3 g/kWh due to a reduction in combustion temperature. Also, EGR dilution enabled more complete combustion by reburning unburned fuel, resulting in lower levels of CH_4, HC, and CO, as well as an improvement in ITE.
5. The optimised DHDF operation at HEF of 76%, by appropriate diesel injection , lower intake air pressure, and EGR addition, resulted in a CO_2 reduction of 23% when compared to CDC, though ITE was lowered by 1.5 percentage points, corresponding to a 3% reduction. Overall GHG emissions (equivalent CO_2) increased by 11% due to the increase in methane slip.

Overall, this experimental study provides a better understanding of the impact of high HEF on performance and all engine-out emissions of a diesel-hythane dual-fuel combustion at low engine load. It is shown that diesel-hythane engine has the potential to contribute to a noticeable CO_2 reduction in the transportation sector if clean energy is employed to produce the hydrogen content of hythane.

Additional studies on different engine speeds and loads are being carried out in order to verify the potential impact of hythane at different engine operating conditions, and the RCCI mode and LIVC will also be investigated to lower exhaust emissions.

References

[1] Exxon Mobil Corporation, "2021 Outlook for Energy: Enery supply," Texas, 2021.

[2] Intergovernmental Panel on Climate Change (IPCC), "IPCC Press Release - Climate change widespread, rapid and intensifying," 2021.

[3] European Commission, "Climate Action - Reducing CO_2 emissions from heavy-duty vehicles," [Online]. Available: https://ec.europa.eu/clima/eu-action/transport-emissions/road-transport-reducing-co2-emissions-vehicles/reducing-co2-emissions-heavy-duty-vehicles_en. [Accessed 21 December 2021].

[4] S. Szwaja, E. Szwaja, S. Rao, M. Szwaja, K. Grab-Rogalinski, J. D. Naber and M. Pyrc, "Influence of exhaust residuals on combustion phases, exhaust toxic emission and fuel consumption from a natural gas fueled spark-ignition engine," *Energy Conversion and Management,* vol. 165, pp. 440-446, 2018.

[5] G. Szabados, A. Bereczky, T. Ajtai and Z. Bozoki, "Evaluation analysis of particulate relevant emission of a diesel engine running on fossil diesel and different biofuels," vol. 161Energy, pp. 1139-1153, 2018.

[6] L. De Simio and S. Iannaccone, "Gaseous and particle emissions in low-temperature combustion diesel–HCNG dual-fuel operation with double pilot injection," *Applied Energy,* vol. 253, 2019.

[7] T. Sandalcı, Ö. Işın, S. Galata, Y. Karagöz and İ. Güler, "Effect of hythane enrichment on performance, emission and combustion characteristics of an ci engine," *International Journal of Hydrogen Energy,* vol. 44, no. 5, pp. 3208-3220, January 2018.

[8] S. L. Kokjohn, R. M. Hanson, D. A. Splitter and R. D. Reitz, "Fuel reactivity controlled compression ignition (RCCI): a pathway to controlled high-efficiency clean combustion," *Internation Journal of Engine Research,* vol. 12, no. 3, pp. 209-226, 2010.

[9] V. B. Pedrozo, I. May, W. Guan and H. Zhao, "High efficiency ethanol-diesel dual-fuel combustion: A comparison against conventional diesel combustion from low to full engine load," *Fuel,* pp. 440-451, 2018.

[10] S. D. Iorio, A. Magno, E. Mancaruso and B. M. Vaglieco, “Analysis of the effects of diesel/methane dual fuel combustion on nitrogen oxides and particle formation through optical investigation in a real engine,” *Fuel Processing Technology,* vol. 159, pp. 200-210, 2017.

[11] M. E. J. Stettler, W. J. B. Midgley, J. J. Swanson, D. Cebon and A. M. Boies, “Greenhouse Gas and Noxious Emissions from Dual Fuel Diesel and Natural Gas Heavy Goods Vehicles,” *Environmental Science and Technology,* vol. 50, no. 4, pp. 2018-2026, 2016.

[12] R. G. Papagiannakis, S. R. Krishnan, D. C. Rakopoulos, K. K. Srinivasan and C. D. Rakopoulos, “A combined experimental and theoretical study of diesel fuel injection timing and gaseous fuel/diesel mass ratio effects on the performance and emissions of natural gas-diesel HDDI engine operating at various loads,” *Fuel,* vol. 202, pp. 675-687, 2017.

[13] A. García, J. Monsalve-Serrano, D. Villalta and R. Sari, “Fuel sensitivity effects on dual-mode dual-fuel combustion operation for different octane numbers,” *Energy conversion and management,* vol. 201, no. 10, 2019.

[14] V. B. Pedrozo, X. Wang, W. Guan and H. Zhao, “The effects of natural gas composition on conventional dual-fuel and reactivity-controlled compression ignition combustion in a heavy-duty diesel engine,” *International Journal of Engine Research,* vol. 23, no. 3, pp. 397-415, 2022.

[15] M. Talibi, R. Balachandran and N. Ladommatos, “Influence of combusting methane-hydrogen mixtures on compression–ignition engine exhaust emissions and in-cylinder gas composition,” *International Journal of Hydrogen Energy,* vol. 42, no. 4, pp. 2381-2396, 2017.

[16] Intergovernmental Panel on Climate Change (IPCC), “Climate Change 2021: The Physical Science Basis - Working Group I Contribution to the Sixth Assessment Report of the Intergovernmental Panel on Climate Change,” 2021.

[17] R. G. Papagiannakis, C. D. Rakopoulos, D. T. Hountalas and D. C. Rakopoulos, “Emission characteristics of high speed, dual fuel, compression ignition engine operating in a wide range of natural gas/diesel fuel proportions,” *Fuel,* vol. 89, no. 7, pp. 1397-1406, 2010.

[18] R. G. Papagiannakis and D. T. Hountalas, “Combustion and exhaust emission characteristics of a dual fuel compression ignition engine operated with pilot Diesel fuel and natural gas,” *Energy Conversion and Management,* vol. 45, no. 18-19, pp. 2971-2987, 2004.

[19] P. K. Bose and D. Maju, “An experimental investigation on engine performance and emissions of a single cylinder diesel engine using hydrogen as inducted fuel and diesel as injected fuel with exhaust gas recirculation,” *International Journal of Hydrogen Energy,* vol. 34, no. 11, pp. 4847-4854, 2009.

[20] Z. Liu and G. A. Karim, “Knock characteristics of dual-fuel engines fuelled with hydrogen fuel,” *Int J Hydrogen Energy,* vol. 20, no. 11, pp. 919-924, 1995.

[21] I. A. Makaryan, I. V. Sedov, E. A. Salgansky, A. V. Arutynunov and V. S. Arutynunov, “A Comprehensive Review on the Prospects of Using Hydrogen–Methane Blends: Challenges and Opportunities,” *Energies,* vol. 15, no. 6, 2022.

[22] G. P. McTaggart-Cowan, S. R. Munshi, S. N. Rogak, P. G. Hill and W. K. Bushe, “Hydrogen-Methane Blend Fuelling of a Heavy-Duty, Direct-Injection Engine,” ASME Internation Mechanical Engineering Congress and Exposition, Washington, 2007.

[23] L. Graham, G. Rideout, D. Rosenblatt and J. Hendren, “Greenhouse gas emissions from heavy-duty vehicles,” *Atmospheric Environment,* vol. 42, no. 19, pp. 4665-4681, 2008.

[24] J. R. Anstrom and K. Collier, “Blended hydrogen-natural gas-fueled internal combustion engines and fueling infrastructure,” in *Compendium of Hydrogen Energy*, Woodhead Publishing Series, 2016, pp. 219-232.

[25] R. Sierens and E. Rosseel, “Variable Composition Hydrogen/Natural Gas Mixtures for Increased Engine Efficiency and Decreased Emissions,” *ASME Journal of Engineering for Gas Turbines and Power,* vol. 122, pp. 135-140, 2000.

[26] K. Collier, N. Mulligan, N. Shin and S. Brandon, “Emission Results from the New Development of A Dedicated Hydrogen-Enriched Natural Gas Heavy Duty Engine,” SAE Technical Paper 2005-01-0235, 2005.

[27] W. Tutak, A. Jamrozik and K. Grab-Rogaliński, “Effect of natural gas enrichment with hydrogen on combustion process and emission characteristic of a dual fuel diesel engine,” *International Journal of Hydrogen Energy,* vol. 45, no. 15, pp. 9088-9097, 2020.

[28] U. Asad and M. Zheng, “Exhaust gas recirculation for advanced diesel combustion cycles,” *Applied Energy,* 2014.

[29] N. Ladommatos, S. Abdelhalim, H. Zhao and Z. Hu, “The Dilution, Chemical, and Thermal Effects of Exhaust Gas Recirculation on Disesel Engine Emissions - Part 4: Effects of Carbon Dioxide and Water Vapour,” SAE Technical Paper 971660, 1997.

[30] R. Hanson, A. Ickes and T. Wallner, “Comparison of RCCI Operation with and without EGR over the Full Operating Map of a Heavy-Duty Diesel Engine,” SAE Technical Paper 2016-01-0794, 2016.

[31] J. F. Larsen and J. S. Wallace, “Comparison of Emissions and Efficiency of a Turbocharged Lean-Burn Natural Gas and Hythane-Fueled Engine,” *ASME Journal of Engineering for Gas Turbines and Power,* vol. 119, pp. 218-226, January 1997.

[32] S. Allenby, W.-C. Chang, A. Megaritis and M. L. Wyszynski, “Hydrogen enrichment: A way to maintain combustion stability in a natural gas fuelled engine with exhaust gas recirculation, the potential of fuel reforming,” *Proceeding of the Institution of Mechanical Engineering, Part D: Journal of Automobile Engineering,* vol. 215, no. 3, pp. 405-418, 2001.

[33] Y. J. Qian, C. J. Zuo, J. Tan and H. M. Xu, “Effect of intake hydrogen addition on performance and emission characteristics of a diesel engine with exhaust gas recirculation,” *Proceeding of the Institution of Mechanical Engineers, Part C: Journal of Mechanical Engineering Science,* vol. 225, no. 8, pp. 1919-1925, June 2011.

[34] S. r. Munshi, C. Nedelcu, J. Harris, T. Edwards, J. Williams, F. Lynch, M. Frailey, G. Dixon, S. Wayne and R. Nine, “Hydrogen Blended Natural Gas Operation of a Heavy Duty Turbocharged Lean Burn Spark Ignition Engine,” SAE Technical Paper 2004-01-2956, 2004.

[35] M. M. Abdelaal and A. H. Hegab, “Combustion and emission characteristics of a natural gas-fueled diesel engine with EGR,” *Energy Conversion and Management,* vol. 64, pp. 301-312, 2012.

[36] Economic Commission for Europe of the United Nations (UN/ECE), “Regulation No 49 - Uniform provisions concerning the measures to be taken against the emission of gaseous and particulate pollutants from compression-ignition engines and positive-ignition engines for use in vehicles,” Official Journal of the European Union, 2013.

[37] J. B. Heywood, Internal Combustion Engine Fundamentals, Second ed., McGraw-Hill Education, 2018.

[38] I. Smith, J. Chiu, G. Bartley, E. Jimenez, T. Briggs and C. Sharp, “Achieving Fast Catalyst Light-Off from a Heavy-Duty Stoichiometric Natural Gas Engine Capable of 0.02 g/bhp-hr NO X Emissions,” SAE Technical Paper 2018-01-1136, 2018.

[39] D. J. Worth, M. E. J. Stettler, P. Dickinson, K. Hegarty and A. M. Boies, “Characterization and Evaluation of Methane Oxidation Catalysts for Dual-Fuel Diesel and Natural Gas Engines,” *Emiss. Control Sci. Technol,* vol. 2, pp. 204-214, 2016.

[40] V. Rapp, N. Killingsworth, P. Therkelsen and R. Evans, “Lean-Burn Internal Combustion Engines,” in *Lean Combustion: Technology and Control*, Second ed., D. Dunn-Rankin and P. Therkelsen, Eds., Academic Press, 2016, pp. 111-146.

[41] W. Guan, X. Wang, H. Zhao and H. Liu, “Exploring the high load potential of diesel–methanol dual-fuel operation with Miller cycle, exhaust gas recirculation, and intake air cooling on a heavy-duty diesel engine,” *International Journal of Engine Research,* vol. 22, no. 7, pp. 2318-2336, 2020.

Appendix

Notation

ATDC	After Top Dead Centre
BTE	Brake Thermal Efficiency
CA10	Crank Angle of 10% Cumulative Heat Release
CA50	Crank angle of 50% Cumulative Heat Release
CA90	Crank angle of 90% Cumulative Heat Release
CA10-CA90	Combustion Duration
CAD	Crank Angle Degrees
CDC	Conventional Diesel Combustion
CH_4	Methane
CI	Compression Ignition
CNG	Compressed Natural Gas
CO	Carbon Monoxide
CO_2	Carbon Dioxide
COV_{IMEP}	Coefficient of Variation of IMEP
DAQ	Data Acquisition
DF	Dual-Fuel

DHDF	Diesel-Hythane Dual-Fuel operation
ECR	Effective Compression Ratio
ECU	Engine Control Unit
EGR	Exhaust Gas Recirculation
EGT	Exhaust Gas Temperature
EU	European Union
GHG	Greenhouse Gases
GWP	Global Warming Potential
HC	Hydrocarbons
HD	Heavy-Duty
HEF	Hythane Energy Fraction
HRR	Heat Release Rate
ICE	Internal Combustion Engine
IMEP	Indicated Mean Effective Pressure
IPCC	Intergovernmental Panel on Climate Change
ISFC	Net Indicated Specific Fuel Consumption
$ISCH_4$	Net Indicated Specific Emissions of Methane
ISCO	Net Indicated Specific Emissions of Carbon monoxide
$ISCO_2$	Net Indicated Specific Emissions of Carbon dioxide
ISHC	Net Indicated Specific Emissions of unburned Hydrocarbon
ISNOx	Net Indicated Specific Emissions of Nitrogen Oxides
ISsoot	Net Indicated Specific Emissions of soot
ITE	Indicated Thermal Efficiency
IVC	Intake Valve Closing
IVO	Intake Valve Opening
LHV	Lower Heating Value
LIVC	Late Intake Valve Closing
$\dot{m}$	Mass Flow Rate
MBF	Mass Fraction Burned
MOC	Methane Oxidation Catalyst
NOx	Nitrogen Oxides
PFI	Port Fuel Injection
P_{int}	Intake Air Pressure
P_{max}	Maximum Average In-cylinder Pressure
PM	Particulate Matter
PRR	Pressure Rise Rate
RCCI	Reactivity-Controlled Compression Ignition
SCR	Selective Catalyst Reduction
SOC	Start of Combustion
SOC-SOI_2	Ignition Delay
SOI_1	Start of Diesel pre-injection
SOI_2	Start of Diesel main injection
TDC	Top Dead Centre
WHSC	World Harmonised Stationary Cycle
WHTC	World Harmonised Transient Cycle
λ	Relative Air-Fuel Ratio
γ	Ratio of Specific Heats